AIAA AVIATION Forum
June 15-19, 2020, VIRTUAL EVENT
AIAA AVIATION 2020 FORUM

10.2514/6.2020-2651

Dynamic Simulation of Vehicle Maneuvers for Loads Analysis

Xiao Jing*, Benjamin P. Berthon†, Luke A. Somers‡, James R. Morgan§, Geoffrey R. Rairigh¶, Darshan Sarojini‖, Evan D. Harrison**, Dimitri N. Mavris††

Aerospace Systems Design Laboratory, School of Aerospace Engineering Georgia Institute of Technology, Atlanta, GA, 30332

Testing critical loads during specific dynamic maneuvers is essential to aircraft structural design, and several such dynamic load cases must be demonstrated during the certification process. A simulation capability is developed in this work to calculate critical loads on the vertical tail of a business jet resulting from yaw maneuvers required for certification. The data produced from these simulations can be used to inform future structural design decisions. Models for the pilot and flight control system are developed to simulate the pilot control actions needed to perform the maneuvers within the boundaries of pilot capabilities and flight control system limits. Aerodynamic and propulsive data are used to calculate the forces and moments on the aircraft and solve the 6-degree of freedom equations of motion to accurately model the aircraft's trajectory. Sectional aerodynamic characteristics of the horizontal and vertical tail are used to calculate the structural loads at each section of the tail. The summation of these forces and moments yields the loads at the vertical tail root, which can be used to assess the structural design of the tail. The simulation is demonstrated on a T-tail business jet with three weight conditions and at flight conditions throughout the flight test envelope. The ultimate loading conditions and the number of control application cycles required to reach ultimate loads at the vertical tail are determined using the maneuver simulation.

I. Introduction

The Federal Aviation Administration (FAA) sets Federal Aviation Regulations (FARs) to place requirements on aircraft design, including structural design, to achieve a desired level of safety and reliability for all certified aircraft. These regulations are intended to account for the worst-case loads to occur in flight. Dynamic load conditions, in particular, often result in the most critical or constraining loads being developed on the structure, and may lead to catastrophic structural failures if unforeseen. A case in point is the loss of American Airlines Flight 587 (an Airbus A300B4 aircraft) due to structural failure of the vertical tail, when the first officer's rapid, and aggressive rudder inputs in response to a wake turbulence encounter resulted in dynamic loads that exceeded the ultimate loads that the tail had been designed for[1].

The FARs permeate throughout the whole design process from the conceptual design to the flight tests, and thus dynamic load conditions must be thoroughly accounted for. Given the monetary cost and time requirements associated with certification programs, a capability that estimates dynamic loads arising from constraining maneuver scenarios earlier in the design process is a definite advantage for the aircraft manufacturer. Such a simulation framework would provide a tool for determining the loads that develop during critical maneuvers for a given design, thus enabling better decision making throughout the design process.

The early preliminary design phase, depicted notionally in Figure 1, offers a large degree of design freedom that may be leveraged by conducting a certification-driven design approach which takes certification requirements into account. Furthermore, a tool which provides additional information regarding structural characteristics arising from dynamic maneuvers can be particularly beneficial. However, the trade-off is that typically only partial information on the aircraft's characteristics is available at the early stage of the design. For example, only lower order fidelity models

*Graduate Research Associate, Aerospace Systems Design Laboratory, Georgia Tech, AIAA Student Member
†Graduate Research Associate, Aerospace Systems Design Laboratory, Georgia Tech
‡Graduate Research Associate, Aerospace Systems Design Laboratory, Georgia Tech, AIAA Student Member
§Graduate Research Associate, Aerospace Systems Design Laboratory, Georgia Tech
¶Graduate Research Associate, Aerospace Systems Design Laboratory, Georgia Tech
‖Senior Graduate Research Associate, Aerospace Systems Design Laboratory, Georgia Tech, AIAA Student Member
**Research Engineer II, Aerospace Systems Design Laboratory, Georgia Tech, AIAA Member
††S.P. Langley Distinguished Regents Professor and Director of ASDL, Aerospace Systems Design Laboratory, Georgia Tech, AIAA Fellow

like beam models for structural analysis and vortex lattice methods for aerodynamics may be available at early portions of the preliminary design.

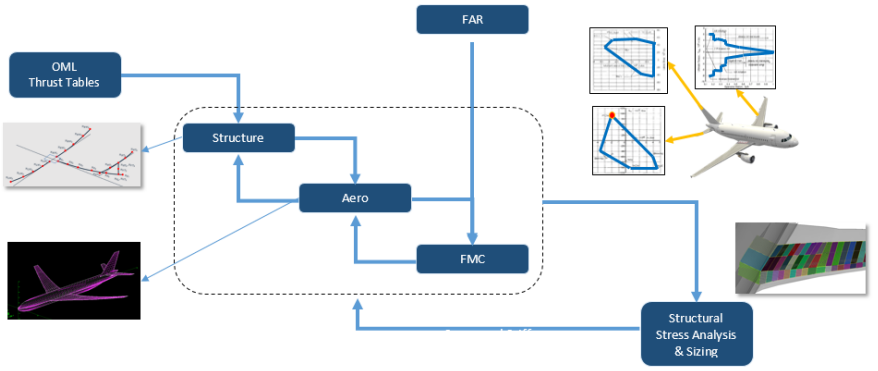

Fig. 1 Notional preliminary design, highlighting key disciplines and analyses

At the end of the detailed design phase, before the manufacturing of the physical aircraft, detailed simulation tools can be more readily applied. At that point in the design, all the detailed geometry of the aircraft, the structure, the aerodynamics performance and the propulsion are typically known. A dynamic maneuver simulation tool can again be leveraged, so as to obtain more accurate estimates the root loads and moments for different components of the aircraft and observe if the structure will fail for a given maneuver. At this late stage of the design process, though, any change in the design as a result of structure failure would be much more costly than in the preliminary design phase.

Once the physical aircraft has been built, aircraft manufacturers perform a series of flight tests to certify the aircraft. Flight Tests are the final step of the validation and can be hazardous for the pilots. A sophisticated simulation tool could provide the pilot with a prior knowledge of the aircraft's behavior during the maneuvers specified by the FAA. This pre-flight simulation could minimize the hazard, time, and hefty cost associated to flight tests.

In prior work [3] [6], a three degree-of-freedom (3-DoF) and a six degree-of-freedom (6-DoF) aircraft simulation capability were developed for accessing dynamic loads developed on the horizontal stabilizer during the maneuver specified in FAR 14 CFR 25.331, and also the sensitivity of these loads to uncertainties in the aircraft aerodynamic characteristics and mass properties was assessed [5].

In this work, the application of a dynamic simulation capability during the late detailed design of an aircraft will be explored more. It will be assumed that various vehicle characteristics, including estimates of the vehicle's Outer Mold Line (OML), aerodynamics, propulsion, and mass properties, are readily available. Rather than consider the full aeroservoelastic problem, this work will decouple the general flexible structural properties and the aerodynamic properties of the vehicle. Instead, we simplified the problem to rigid-body flight dynamics in the paper. While future application of the methods developed in this tool would allow for design iteration, the focus of this work will be limited to the evaluation of critical maneuver loads.

The maneuver considered in this paper is that specified in FAR 14 CFR 25.351, which describes a yaw maneuver condition which the aircraft structure must be able to withstand [2]. This maneuver scenario may result in the critical design loads for the vertical tail and the maximum hinge moment for the rudder. This work builds upon and extends the simulation framework developed by Goron et al [3], which modeled the checked pitch maneuver described in 14 CFR 25.331. The maneuvers considered in this study are the rudder kick maneuver outlined in 14 CFR 25.351 as well as a more stringent case known as "walking the rudder"[2][1]. For both maneuvers, this simulation will be used to determine vertical stabilizer root loads. The simulation will model a representative business jet from an aircraft manufacturer's product line and will run instances of these maneuvers at several different points in the flight envelope. The critical cases resulting in the highest loads will be examined, and the relevant implications to the structural design process will be discussed. The results to be presented in this paper will be suitably modified or redacted where necessary in order to protect proprietary data corresponding to this aircraft's aerodynamics, mass properties, geometry, and performance envelope.

II. Technical approach

In order to determine the structural loads, the system needs to be divided in different subsystems, which are described in the global architecture depicted in Figure 2. The main blocks are the Maneuver, Aerodynamic Model, Dynamic Simulation and Structural Loads blocks. The Maneuver block will define the desired maneuver from the FAR, simulate the pilot action and then achieve the desired state thanks to a controller. The Aerodynamic Model block will calculate the propulsive and aerodynamic forces and moments, obtained from the aircraft manufacturer data. The Dynamic Simulation block will update the states of the aircraft using data gathered from other components during the simulation as well as the mass properties. Finally, the Structural Loads block will calculate the loads on the vertical tail at each step of the simulation.

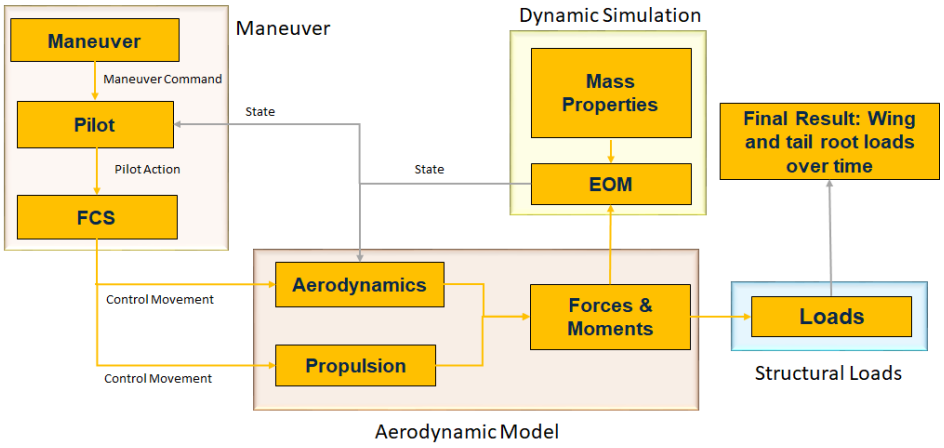

Fig. 2 Overview of simulation system architecture

A. Maneuver

1. Maneuver Definition

As mentioned previously, the maneuver considered in this paper are the rudder kick and walking the rudder maneuvers. The rudder kick maneuver involves a single, sudden, full-scale deflection of the rudder control to one side, followed by a release of that control back to neutral after achieving a steady sideslip angle. Figure 3 shows the rudder deflection, the sideslip angle, and the derivative of sideslip angle during a notional rudder kick maneuver. In characterizing this particular maneuver consideration is given to appropriate timing for the release of the rudder deflection. Both the sideslip and sideslip derivative signals show oscillatory behaviors that settle, but the sideslip's signal has an offset from zero: the nonzero sideslip during the rudder full deflection stage. Because of this, additionally logic would be necessary to calculate the sideslip steady state offset in addition to calculating the settling time, so it is much simpler to just use the derivative of sideslip, which has no steady state offset, as the condition for defining the release of the rudder during this maneuver.

The other maneuver that was investigated is the walking the rudder maneuver. This maneuver is not defined by FAR and is not commonly used in American flight testing; instead, walking the rudder is defined by the European Aviation Safety Agency (EASA). The maneuver requires that from a steady and level flight the pilot inputs a maximum rudder deflection in one direction. Once the aircraft reaches a maximum steady sideslip angle, the rudder deflection is reversed to be the maximum in the other direction. This is repeated five more times for a total of six rudder deflections, or three cycles.

2. Pilot control

Once the Maneuver Block determines a desired deflection angle, it is injected to the Pilot Block. Here, there are several blocks that work to convert the often-idealized maneuver output into actionable pilot forces. For instance, the Maneuver block can output smooth or discontinuous deflection commands, suddenly jumping between values. It also does not account for the physical forces applied to the control surfaces or pilot controls. In the present formulation the

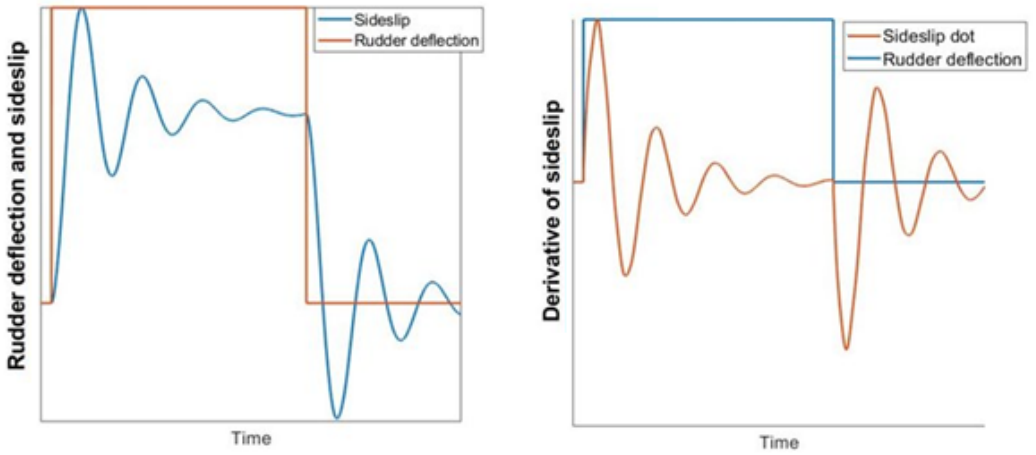

Fig. 3 Notional rudder kick time response

Pilot block is used to account for these practical considerations. As shown by Figure 4, the Pilot block will take in a deflection command, compare it to the current deflection for that surface, then apply a PID transfer function to those values to receive a corresponding pilot force on the controls.

Fig. 4 Pilot forces implementation

In order to obtain realistic and stable pilot behavior, these pilot gains must be tuned. With values for proportional, integral, and derivative gains in each control axis, there are a total of nine gains to tune. If one gain is too high or too low, the aircraft may become unstable due to the PID response. With a general intuition of the relationships between proportional, integral, and derivative gains, initial guesses for gain values could be made and refined over successive iterations; however, this is quite a slow process as the simulation executes in slower than real time and takes time to initialize.

As an aid to help obtain stable behavior with the pilot gains, additional proportional-derivative (PD) controllers were added into the Maneuver block to drive the commanded deflections of roll and pitch to the trim states. This helps to ensure stable aircraft motion throughout the maneuvers as a sinlge controller is actively controlling large deflections: the yaw controller, which is the controller primarily focused on in our two maneuvers.

3. Flight Control System Dynamics

After calculating the pilot forces, the Flight Control System block (FCS) is used to translate the pilot forces into control surface deflections. It was implemented following the FCS developed for elevator deflection in [3]. This system for the elevator deflection is shown in Figure 5. It consists of mechanical linkages between the pilot actions and the actuator deflections. A hydraulic actuator is also present which helps the pilot to deflect the control surfaces.

Second order ordinary differential equation are derived for the elevator deflection, the rudder deflection, and the aileron deflection where $m_{(.)}$ is the effective translating mass of the control system, $c_{l_{(.)}}$, $c_{r_{(.)}}$ the translational and rotational friction loss coefficients, $k_{(.)}$ the proportional factor of the hydraulic booster, and $G_{(.)}$ the gearing ratio. Additional details can be found in [3].

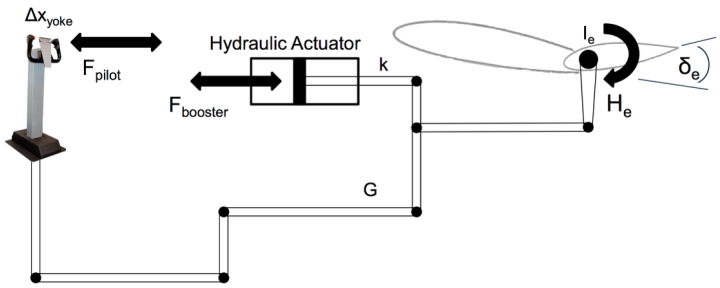

Fig. 5 Flight control system

$$\left(I_e + \frac{m_e(1+k_e)}{G_e^2}\right)\ddot{\delta_e} + \left(c_{re} + \frac{c_{le}(1+k_e)}{G_e^2}\right)\dot{\delta_e} = F_{pilot_e}\left(\frac{1+k_e}{G_e}\right) + H_e \tag{1}$$

$$\left(I_a + \frac{m_a(1+k_a)}{G_a^2}\right)\ddot{\delta_a} + \left(c_{ra} + \frac{c_{la}(1+k_a)}{G_a^2}\right)\dot{\delta_a} = F_{pilot_a}\left(\frac{1+k_a}{G_a}\right) + H_a \tag{2}$$

$$\left(I_r + \frac{m_r(1+k_r)}{G_r^2}\right)\ddot{\delta_r} + \left(c_{rr} + \frac{c_{lr}(1+k_r)}{G_r^2}\right)\dot{\delta_r} = F_{pilot_r}\left(\frac{1+k_r}{G_r}\right) + H_r \tag{3}$$

$H_{(.)}$ is the hinge moment of the actuator and can be determined from a set of look-up tables. The hinge moment of the rudder H_r depends on the sideslip β and the rudder deflection δ_r. The hinge moment of the ailerons H_a depends on the aileron deflections $\delta_{a_{1/2}}$. The hinge moment of the elevator H_r depends on the tail angle of attack α_{tail}, the elevator deflection δ_r and the trim tab deflection δ_{tab}.

B. Aerodynamics

The study of the yaw maneuvers requires to obtain all aerodynamic forces and moments. The basis of the aerodynamic model for this work is a series of aerodynamic tables which provide aerodynamic coefficients in the wind frame. The different states required to query these tables are the Mach number, the angle of attack α, the sideslip angle β, the actuators deflections (rudder δr, elevator δe and ailerons δail) and the attitudes (roll p, pitch q, yaw r). Each aerodynamic coefficient depends on these states. The aerodynamic forces and moments are modeled as the sum of the tail-off contribution and the isolated tail contribution.

The aerodynamic coefficients of the tail will depend on the local angle of attack and sideslip angle. The angle of attack of the tail depends on the aircraft angle of attack α, the stabilizer setting angle i_t, the downwash ϵ and the incremental angle generated due to the pitch rate q and V the airspeed. The sideslip angle of the tail depends on the aircraft sideslip β, the incremental angles generated due to the roll rate p and the yaw rate r and V the airspeed.

$$\alpha_{tail} = \alpha + i_t - \epsilon + \frac{ql}{V}$$
$$\beta_{tail} = \beta + \frac{z_{VT} - z_{CG}}{V}p + \frac{x_{VT} - x_{CG}}{V}r$$

The drag D, sideforce and lift coefficients can be written with the contributions of the states as :

$$C_D = C_{D_{wing}}(M, \alpha, \beta, \delta_{ail1}, \delta_{ail2}) + C_{D_{tail}}(M, \alpha_{tail}, \beta_{tail}, \delta_e, \delta_r)$$

$$C_Y = C_{Y_{wing}}(M, \alpha, \beta, \delta_{ail1}, \delta_{ail2}) + C_{Y_{tail}}(M, \alpha_{tail}, \beta_{tail}, \delta_e, \delta_r)$$
$$C_L = C_{L_{wing}}(M, \alpha, \beta, \delta_{ail1}, \delta_{ail2}) + C_{L_{tail}}(M, \alpha_{tail}, \beta_{tail}, \delta_e, \delta_r)$$

The rolling, pitching and yawing coefficients can be written with the contributions of each state as :

$$C_l = C_{l_{wing}}(M, \alpha, \beta, \delta_{ail1}, \delta_{ail2}) + C_{l_{tail}}(M, \alpha_{tail}, \beta_{tail}, \delta_e, \delta_r)$$

$$C_m = C_{m_{wing}}(M, \alpha, \beta, \delta_{ail1}, \delta_{ail2}) + C_{m_{tail}}(M, \alpha_{tail}, \beta_{tail}, \delta_e, \delta_r)$$
$$C_n = C_{n_{wing}}(M, \alpha, \beta, \delta_{ail1}, \delta_{ail2}) + C_{Ln_{tail}}(M, \alpha_{tail}, \beta_{tail}, \delta_e, \delta_r)$$

The elevator deflection is the same for both elevators whereas the aileron deflections are different, explaining the subscripts 1 and 2 for δ_{ail}. The aerodynamic tables are interpolated to get each aerodynamic contribution $C_{(.)_{tail-off/tail}}$.

The drag D, the sideslip Y, the lift L, the rolling M_l, pitching M_m, yawing M_n moments can be obtained as :

$$D = \overline{q}.S.C_D \qquad M_l = \overline{q}.S.MAC.C_l$$
$$Y = \overline{q}.S.C_Y \qquad M_m = \overline{q}.S.MAC.C_m$$
$$L = \overline{q}.S.C_L \qquad M_n = \overline{q}.S.MAC.C_n$$

where $\overline{q}$ is the dynamic pressure, S the planform area of the wing and MAC the mean aerodynamic chord.

C. Propulsion

Contrary to aerodynamic forces and moments, the thrust and the generated moment are directly written in the body frame. The thrust T is parallel to the body-fixed x-axis and modeled using a linear relationship between the minimum thrust T_{min} and the maximum thrust T_{max}, which are given by tables and depend on the Mach number M and the altitude h. Then, the thrust can be written as :

$$\overrightarrow{T}(\tau, h, M) = [T_{min}(h, M) + \tau(T_{max}(h, M) - T_{min}(h, M))]\overrightarrow{e}_{x_{body}} \qquad \text{where } \tau \in [0, 1] \text{ the throttle setting}$$

The moment due to the thrust about the reference point is calculated with the cross product of the thrust and $\overrightarrow{r}$ the vector from the reference point and the thrust application point.

$$\overrightarrow{M_T} = \overrightarrow{r} \times \overrightarrow{T}$$

D. Equation of motions

In order to form the total external forces and moments applied on the aircraft, the aerodynamic forces and moments are moved from the wind frame to the body frame (Figure 6) and then, they are respectively added to the thrust and the moment due to the thrust. Using known mass properties, the equations of motion can be fully written in the body frame at a reference point, different than the center of gravity because the latter changes due to fuel consumption or fuel transfer. They are given in Equation 4 and 5.

$$\overrightarrow{F}_{total} = m[\dot{\overrightarrow{V}}_0 + (\overrightarrow{\omega} \times \overrightarrow{V}_0) + \ddot{\overrightarrow{r}}_G + (\dot{\overrightarrow{\omega}} \times \overrightarrow{r}_G) + 2(\overrightarrow{\omega} \times \dot{\overrightarrow{r}}_G) + (\overrightarrow{\omega} \times (\overrightarrow{\omega} \times \overrightarrow{r}_G))] \tag{4}$$
$$\overrightarrow{M}_{total} = \bar{\bar{I}}\dot{\overrightarrow{\omega}} + (\overrightarrow{\omega} \times \bar{\bar{I}}\overrightarrow{\omega}) + m\overrightarrow{r}_G \times (\dot{\overrightarrow{V}}_0 + (\overrightarrow{\omega} \times \overrightarrow{V}_0)) \tag{5}$$

where $\overrightarrow{V}_0 = u, v, w^T$ the velocity of the reference point O, $\overrightarrow{\omega}_0 = p, q, r^T$ the angular velocity and $\bar{\bar{I}}$ the inertia tensor written in the body frame.

E. Trim

Trimming the aircraft for a steady and level flight is a required pre-processing step before conducting maneuver simulations. Trimming means that, for a given state (Mach and altitude) a stable configuration must be found so that the sum of forces and moments exerted on the aircraft cancel out. This process is described in Figure 7. The goal is to solve a minimization problem by minimizing the six forces and moments components by leveraging the use of six independent variables: angle of attack, sideslip, throttle setting, and the deflection of the elevator, rudder and aileron. The optimization scheme used was a Levenberg-Marquardt algorithm and the cost function was the sum of the normalized forces and moments. For a symmetric aircraft with a steady and level flight configuration, only the angle of attack, the throttle setting and the elevator deflection need to be trimmed to minimize the pitch as well as the vertical and horizontal acceleration. The trim configurations obtained for a set of different states can be seen on Figures 8 to 10.

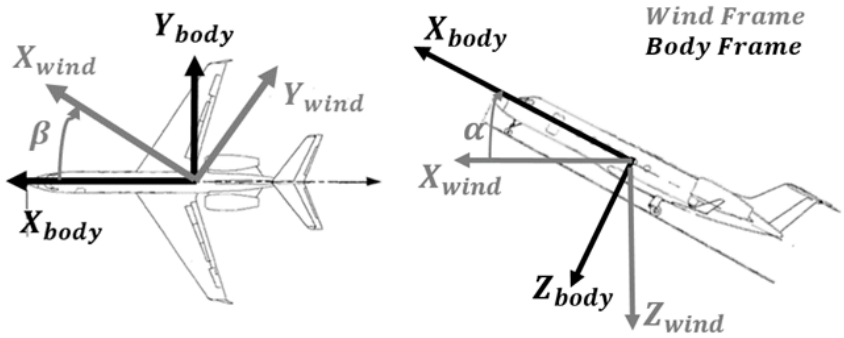

Fig. 6 Wind and body frames

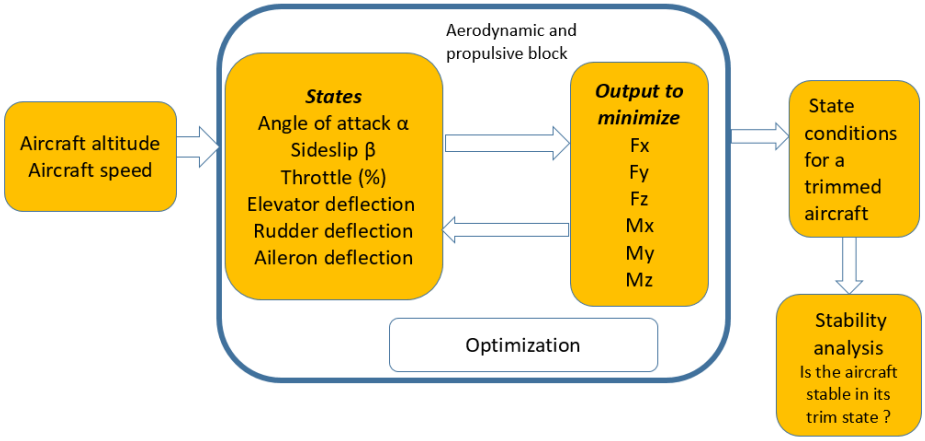

Fig. 7 Trimming flowchart

F. Structural loads

The main quantities of interest for this study are the structural loads at the root of the vertical tail during the given maneuver. To obtain these loads, the vertical tail has been discretized into a set of panels of known mass and moments of inertia about the panel CG. The forces and moments acting on any given panel are assumed to consist of aerodynamic forces and moments, control surface forces and moments, gravity forces, and structural loads. The acceleration associated with any point on a panel is assumed to be consistent with the rigid body assumption, this acceleration constraint is sometimes characterized as the fictitious "inertia force" and "inertia moment".

The aerodynamic and control loads acting at specific points along these panels are known as a function of the aircraft state. Taking forces and moments about the panel root yields the dynamic equilibrium equations:

$$\vec{F}_{total} = \vec{F}_r^{(k)} + \vec{F}_r^{(k+1)} + \vec{F}_a^{(k)} + \vec{F}_g^{(k)} + \vec{\Delta F}_{a_{\delta,e}}^{(k)} = m^{(k)}\vec{a}_{cg}^{(k+1)} = -\vec{F}_i^{(k)} \tag{6}$$

$$\vec{M}_{total} = \vec{M}_r^{(k+1)} + \vec{M}_r^{(k)} + \vec{r}_r^{(k)} \times \vec{F}_r^{(k)} + \vec{M}_a^{(k)} + \vec{r}_a^{(k)} \times \vec{F}_a^{(k)} + \vec{r}_{cg}^{(k)} \times \vec{F}_g^{(k)} + \vec{r}_{a_{\delta e}}^{(k)} \times \vec{\Delta F}_{a_{\delta,e}}^{(k)} \tag{7}$$

$$= I_{panel,cg}^{(k)}\vec{\omega} + \vec{w} \times \vec{I}_{panel,cg}^{(k)}\vec{\omega} \tag{8}$$

Where the acceleration of the panel root is known from the known aircraft level velocity, acceleration, and angular rates along with the known location of the panel root. To solve for the root loads, it is assumed that the structural loads at the vertical tail tip are identically zero. Thus, for the first panel, the only unknown in the dynamic equilibrium equations are the reaction forces and moments at the 2nd panel boundary can be determined. Continuing in this fashion, the kth

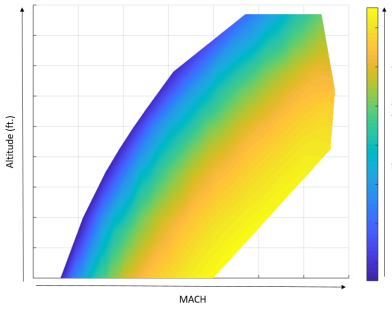

Fig. 8 Trim state for the elevator's angle deflection

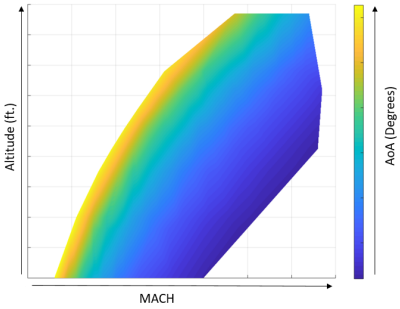

Fig. 9 Trim state for the angle of attack

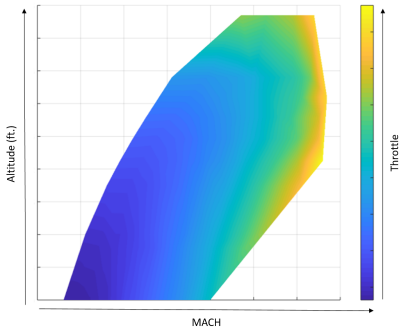

Fig. 10 Trim state for the throttle setting

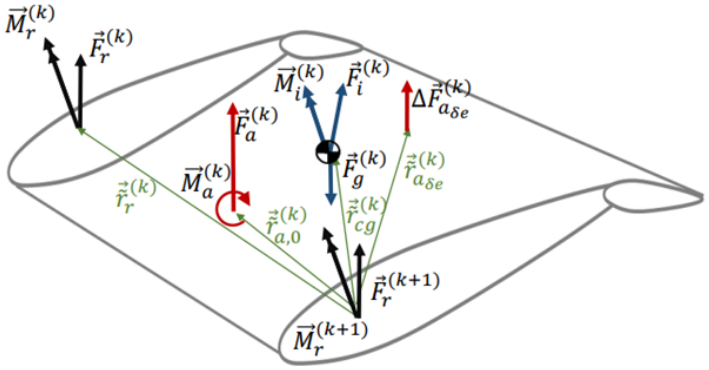

Fig. 11 Tail panel free body diagram

panel structural loads are known for a given panel, allowing for the k+1th panel structural loads to be determined. The loads are calculated in sequence from the vertical tail tip to the vertical tail root.

III. Results

After completing the linear interpolation, maneuver definition, and structural loads buildup, the simulator could be run to obtain time histories of the horizontal and vertical tail root loads as a function of time.

For each flight condition specified in terms of a mach number and altitude, an initial trim condition was computed, which served as the condition from which to propagate the equations of motion. At time t=3 seconds, the command would be applied to the controller. At each instant in time, the forces and moments at the tail root were computed using the method previously described. The resulting time history of tail root loads for each mach/altitude condition were stored for further analysis.

A sample time history showing the rolling moment and side force acting at the root of the vertical tail during a rudder kick maneuver is shown in (figure 12). For reference, the sideslip angle is also included.

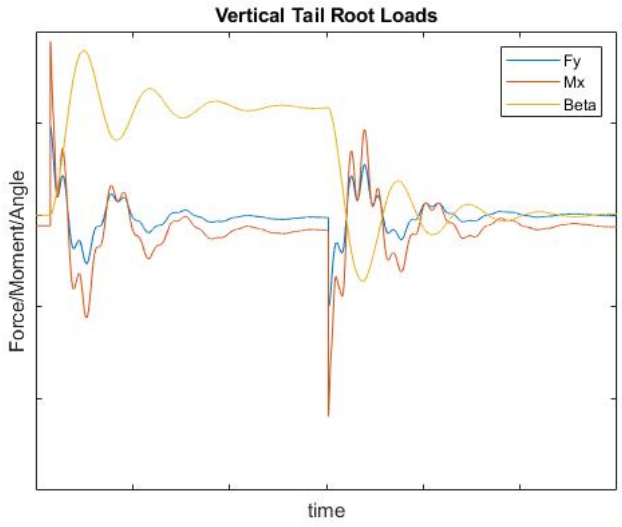

Fig. 12 Vertical tail root loads time history

From Figure 12, one can see that there are spikes in the root loads at the approximate time when the rudder deflection is applied and when the rudder is released. The directions of the side force and rolling moment root forces are in the same direction, which one would expect for a rudder kick maneuver. As the aircraft approaches a steady condition, the root loads are damped out to the previous steady state values. Figure 12 shows the time history of these root loads for a particular flight condition in terms of a Mach number and altitude. Similar plots exist for every feasible combination of Mach number and altitude.

By taking the maximum load value in each body axis direction for each flight condition, heatmaps of the maximum expected root loads vs flight condition for the rudder kick maneuver can be created, as depicted by Figure 13. Note that no distinction was made between load directions, the maximum magnitude load was plotted on the root load buildups. A similar approach may be used to generate heatmaps of maximum positive and negative loads, which may be important to structural designers.

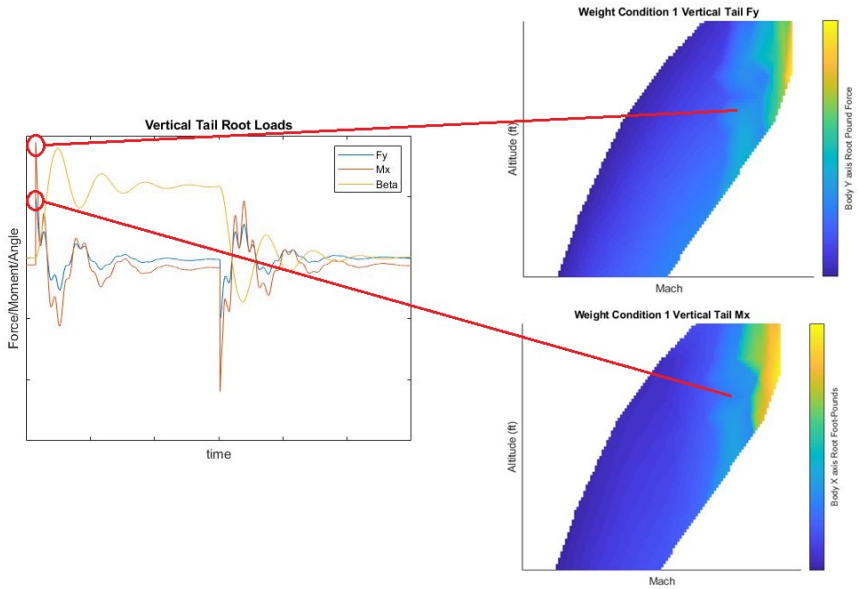

Fig. 13 Root load buildup

Some sample heatmaps for the vertical tail root loads during the rudder kick maneuver in weight condition 2 are shown in Fig. 14. Note that the force/moment data is shown on a logarithmic scale to highlight trends. The force/moment values and their associated Altitude and Mach values have been removed to protect proprietary data.

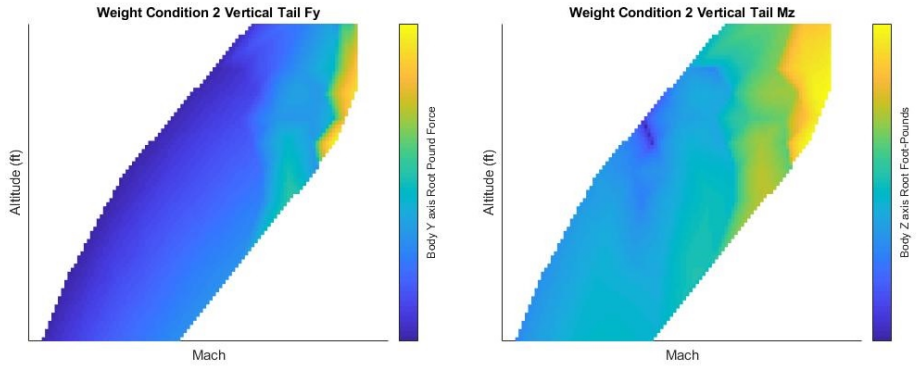

Fig. 14 Rudder kick vertical tail peak root load heatmap examples

We can see that in general, the peak root loads in the vertical tail tends to increase with mach number as one would expect. In the case of the side force Fy, the force decreases with altitude for a given mach number. In these conditions, the dynamic pressure is greater, resulting in larger aerodynamic loads from a given control surface deflection. The critical point in terms of maximum tail root loads occurs at the highest mach number considered at the lowest altitude for the given mach number.

IV. Conclusion and Future work

This paper shows the results and analysis of the simulation of critical loads on the vertical tail. This approach is particularly useful in certifying for yaw maneuvers. The simulation outputs root loads across the entire flight envelope; the maximum of these loads are identified as the critical loads for each maneuver defined by the FAR. The process of creating a complete tool contains three steps, the first of which was completed and documented in this paper: a 6 DoF framework identifies roots loads for the rudder kick maneuver and the walking the rudder maneuver.

The next step is to implement all maneuvers as defined by the FAR in order to obtain the complete critical load envelope. Finally, the last step is to continue developing the global optimized framework, enabling structural and aerodynamic design optimization using a feedback loop.

Acknowledgements

The authors wish to express their gratitude to Gulfstream Aerospace Corporation for the data sources and financial support to this research project.

References

[1] "Aircraft Accident Report: In-Flight Separation of Vertical Stabilizer. American Airlines Flight 587: Airbus Industrie A300-605R, N14053. Belle Harbor, New York. November 12, 2001." , 2004. National Transportation Safety Board (NTSB), NTSB/AAR-04/04.

[2] "Code of Federal Regulations, Title 14, Part 25 (14 CFR 25) - Airworthiness Standards: Transport Category Airplanes," , 2018. Federal Aviation Administration (FAA), US Department of Transportation (USDOT).

[3] Goron, G., Duca, R., Sarojini, D., Shah, S., Chakraborty, I., Briceno, S., , and Mavris, D.,*"A Simulation-Based Framework for Structural Loads Assessment during Dynamic Maneuvers."* AIAA aviation conference 2017.

[4] Etkin, B.,*"Dynamics of Flight: Stability and Control"*, John Wiley and Sons Australia Limited, 1982.

[5] Duca, R., Sarojini, D., Blomer, S., Chakraborty, I., Briceno, S., and Mavris, D. N.,*"Effects of Epistemic Uncertainty on Structural Loads During Dynamic Maneuvers."* AIAA Science and Technology Forum and Exposition (AIAA SciTech Forum) 2018.

[6] Sarojini, D., Duca, R., Solano, H., Chakraborty, I., Briceno, S., Mavris, D.,*"Framework to Assess Effects of Structural Flexibility on Dynamic Loads Developed in Maneuvering Aircraft."* AIAA aviation conference 2018.